AMERICAN ACADEMY OF OPHTHALMOLOGY®

Bruch's Membrane Calcification in Pseudoxanthoma Elasticum

Comparing Histopathology and Clinical Imaging

Sara Risseeuw, MD, PhD,[1] Matthew G. Pilgrim, PhD,[2] Sergio Bertazzo, PhD,[3] Connor N. Brown, PhD,[2] Lajos Csincsik, PhD,[2] Sarah Fearn, PhD,[4] Richard B. Thompson, PhD,[8] Arthur A. Bergen, PhD,[5,6] Jacoline B. ten Brink, BAS,[5] Elod Kortvely, PhD,[7] Wilko Spiering, MD, PhD,[9] Jeannette Ossewaarde–van Norel, MD, PhD,[1] Redmer van Leeuwen, MD, PhD,[1] Imre Lengyel, PhD[2,3]

Purpose: To investigate the histology of Bruch's membrane (BM) calcification in pseudoxanthoma elasticum (PXE) and correlate this to clinical retinal imaging.

Design: Experimental study with clinicopathological correlation.

Subjects and Controls: Six postmortem eyes from 4 PXE patients and 1 comparison eye from an anonymous donor without PXE. One of the eyes had a multimodal clinical image set for comparison.

Methods: Calcification was labeled with OsteSense 680RD, a fluorescent dye specific for hydroxyapatite, and visualized with confocal microscopy. Scanning electron microscopy coupled with energy-dispersive x-ray spectroscopy (SEM-EDX) and time-of-flight secondary ion mass spectrometry (TOF-SIMs) were used to analyze the elemental and ionic composition of different anatomical locations. Findings on cadaver tissues were compared with clinical imaging of 1 PXE patient.

Main Outcome Measures: The characteristics and topographical distribution of hydroxyapatite in BM in eyes with PXE were compared with the clinical manifestations of the disease.

Results: Analyses of whole-mount and sectioned PXE eyes revealed an extensive, confluent OsteoSense labeling in the central and midperipheral BM, transitioning to a speckled labeling in the midperiphery. These areas corresponded to hyperreflective and isoreflective zones on clinical imaging. Scanning electron microscopy coupled with energy-dispersive x-ray spectroscopy and TOF-SIMs analyses identified these calcifications as hydroxyapatite in BM of PXE eyes. The confluent fluorescent appearance originates from heavily calcified fibrous structures of both the collagen and the elastic layers of BM. Calcification was also detected in an aged comparison eye, but this was markedly different from PXE eyes and presented as small snowflake-like deposits in the posterior pole.

Conclusions: Pseudoxanthoma elasticum eyes show extensive hydroxyapatite deposition in the inner and outer collagenous and elastic BM layers in the macula with a gradual change toward the midperiphery, which seems to correlate with the clinical phenotype. The snowflake-like calcification in BM of an aged comparison eye differed markedly from the extensive calcification in PXE.

Financial Disclosure(s): Proprietary or commercial disclosure may be found in the Footnotes and Disclosures at the end of this article.

Supplemental material available at www.ophthalmologyscience.org.

In patients with pseudoxanthoma elasticum (PXE), biallelic mutations of the *ABCC6* gene lead to ectopic calcification of elastic fibers in the skin, vasculature, and Bruch's membrane (BM) in the eyes.[1,2]

Bruch's membrane is a 2- to 5-μm thin layer of extracellular matrix between the choroid and the retinal pigment epithelium (RPE).[3] Bruch's membrane consists of 3 layers; these include an elastic layer that is bordered by the inner and outer collagenous layers.[4–7] The RPE basal lamina and the choriocapillaris basal lamina deliminate BM from the RPE and the choriocapillaris, respectively.[8,9] Bruch's membrane allows the diffusion of biomolecules, such as oxygen and nutrients from the choroidal blood flow, and metabolic waste and growth factors (such as VEGF) from the RPE.[10] Diffusion largely depends on the hydrostatic pressure on both sides of BM, and the concentrations of the molecules but also depends on permeability of BM.[9,11] Besides facilitating diffusion, BM also serves as a support layer for RPE cell adhesion and restricts the movement of cells between the retina and choroid.[10]

https://doi.org/10.1016/j.xops.2023.100416
ISSN 2666-9145/23

The structure and properties of BM change with increasing age. Throughout life, BM doubles in thickness due to cross-linking of the collagen fibers and accumulation of advanced glycation end products,[12] lipids, and waste products; also, the continuous turnover of the extracellular matrix might be affected.[3,8,10,13–15] Moreover, mineralization in BM, especially calcification of the elastic layer, is common with aging and reduces permeability.[14,16–19] Also, the accumulation of lipids is assumed to increase the hydraulic resistance of BM, thereby impeding diffusion.[20]

Changes in the structure or properties of BM often play a role in diseases of the outer retina or choroid, for example in age-related macular degeneration (AMD), which is the leading cause of visual impairment in Europe.[21,22] The decreasing permeability in the aging BM might lead to an accumulation of RPE-secreted lipids to form a "lipid wall."[10,23] A buildup of these lipids can be seen as soft drusen, which are important predictors for late-stage AMD.[24]

Furthermore, calcification of BM reduces its elasticity, making the membrane more prone to focal breaks, and allowing the ingrowth of vessels from the choroid, causing choroidal neovascularization.[25]

In patients with PXE, the calcification of BM is likely caused by lower-than-normal levels of systemic inorganic pyrophosphate, a potent inhibitor of ectopic calcification.[26] Clinically, BM calcification in PXE patients is visible as an increased fundus reflex. Especially in younger patients, the increased fundus reflex often has a mottled and speckled pattern, the so-called peau d'orange is assumed to be the visible transition zone between the calcified BM and the less-affected BM in the retinal periphery.[27] Within the area of peau d'orange, BM calcification slowly becomes confluent and progresses centrifugally during life.[28] Nearly all patients present with angioid streaks, which are defects in BM and can be seen as irregular jagged break lines that spread from the optic disc to the periphery.[29] It is assumed that angioid streaks develop because of mechanical stress exerted on the eye by eye movements, resulting in the fracture of the brittle, calcified BM.[30,31] In a later stage of PXE, late-phase indocyanine green angiography (ICGA) reveals a hypofluorescent area with speckled borders in the central retina.[27] This area is only visible in PXE patients aged $>$ 30 years and seems to depend on the degree of BM calcification.[28] The mechanism underpinning indocyanine green (ICG) hypofluorescence is yet unknown, but reduced uptake of ICG dye by the RPE cells, either due to reduced BM permeability or subclinical damage of RPE cells, might be involved.[32,33] Both the increased fundus reflex and the ICGA hypofluorescent area likely represent different stages of BM disease and seem to progress slowly during life within a predetermined area of the fundus.[27,28]

Little to no detailed information is available on the underlying histopathological changes in BM that underpin the clinical features of PXE on retinal imaging, such as peau dórange, ICGA hypofluorescence, and the predetermined area of BM calcification. These histology–imaging correlations and detailed characteristics of BM calcification in PXE are essential to improve effectiveness of clinical monitoring and the development of image-based biomarkers. Also, gaining insight into BM calcification phenotypes such as aging-associated BM calcification is highly valuable for understanding "normal" age-related BM calcification, which occurs in the majority of the aging population,[14] compared with excessive BM calcification.

In this study, we investigated the characteristics of BM calcification in human eyes with PXE and comparison eyes without PXE. We use a whole-mounted eye approach for a detailed topographical comparison between histopathological changes and clinical retinal imaging. We employed whole-eye cross sections and molecular imaging to gain a better understanding of the structural and elemental characteristics of BM calcification.

Methods

Tissue Origins

In total, 1 control eye of an anonymous donor and 6 eyes of 4 PXE patients were obtained. Donor 1 and 2 were PXE patients at the Dutch National Expertise Center for PXE, Utrecht, the Netherlands, whereas the eyes of donors 3 and 4 were obtained through the Netherlands Institute for Neuroscience, Amsterdam, the Netherlands. The control eye with no known systemic or retinal disease was obtained from University College London and Moorfields Eye Hospital Tissue Repository. The time from death to preservation was unknown in 2 PXE patients and was 24 hours and 30 hours in the other 2 PXE patients. More details on the donor eyes are presented in Table S1 (available at www.ophthalmologyscience.org). Written informed consent for the use of the eye tissue was obtained in each case. This study adhered to the tenets of the Declaration of Helsinki and the work on the cadavers was approved by the research ethics committee of the Faculty of Medicine, Health & Life Sciences of Queens University Belfast.

Tissue Preparation

Cadaveric eyes were enucleated and fixed in 4% paraformaldehyde solution. Subsequently, the anterior segment of each eye, including the lens and cornea, was removed through a circular cut through the limbus.

To generate consecutive cross sections of the left eyes of donors 1 and 2, the posterior segment was embedded in paraffin wax using a Leica ASP300S tissue processor. Cross sections that were approximately 7 μm thick were generated by sectioning the embedded eye using an RM2225 microtome. Sections were then deparaffinized using a series of xylene and ethanol dilutions. In short, tissues were immersed in xylene for 5 minutes (repeated 3 times), followed by rehydration in a graded ethanol series (100%, 100%, 90%, 90%, 70%, and 70%). Glass slides with tissues were then immersed in distilled water.

Whole mounts (all 5 right eyes) were prepared after the removal of the vitreous humor. Several incisions were made from the *ora serrata* toward the optic nerve head. A circular incision around the optic nerve head allowed the removal of the sclera from the chorioretinal complex. The choroid and neurosensory retina were then separated and flat-mounted on glass slides. The choroidal samples were mounted with BM on the top, and the samples of the neurosensory retina were exposed with the photoreceptors on the top (Fig S1, first column, available at www.ophthalmologyscience.org).

Tissue Analyses

OsteoSense 680RD Staining and Microscopy. Calcification on whole-mounts and cross sections were incubated with OsteoSense

680EX (0.002 nM/μL in Tris buffered saline; Perkin Elmer) for 20 minutes, then washed for 5 minutes (repeated 3 times) with phosphate buffered saline. Samples were then counterstained with Hoechst 33342 (1:10 000) (Thermo Fisher Scientific) to visualize cell nuclei. Biotinylated lectin agglutinin-I (1:00; Vector Laboratories) and AlexaFluor 568 streptavidin conjugate secondary antibody (1:200; Thermo Fisher Scientific) were used to visualize the vascular endothelium.

Samples were mounted in 70% glycerol before coverslips were applied and sealed with nail varnish. An inverted scanning confocal microscope (SP8; Leica Biosystems) was used to image fluorescence labeling. For OsteoSense 680EX, the excitation wavelength was 638 nm, and the detected emission wavelength was 643 to 700 nm. For Hoechst 33342, the excitation wavelength was 405 nm, and the emission was detected at 410 to 484 nm. AlexaFluor 568 was detected at excitation wavelength 552 nm, and emission was detected at 575 to 619 nm.

Scanning Electron Microscopy. Glass slides with fixed and dehydrated human cadaveric eye tissues were mounted on to aluminum stubs (Agar Scientific) using conductive adhesive tabs. To ensure conductivity of the sample, adhesive copper tape (Agar Scientific) was used to form a conductive bridge between the surface of the glass slide and the underside of the aluminum stub. Conductive silver paint (Agar Scientific) was applied to the underside edge and the surface of the slide to further ensure conductivity. Samples were sputter-coated with 1 nm of gold or with a 5-nm carbon layer.

Scanning electron micrographs were generated using a Hitachi S-3400N (Hitachi) or an LEO 1530 (Carl Zeiss) microscope. Secondary electron micrographs and backscattered electron micrographs were generated using an accelerating voltage of 10 kV, and a working distance of 10.0 mm. Density-Dependent Color Scanning Electron Microscopy (DDC-SEM) is obtained by a combination of secondary electrons and back-scattering electron images.[34]

Energy-dispersive x-ray Spectroscopy. Energy-dispersive x-ray spectroscopy was performed using the AZtec nano analysis system (Oxford Instruments), coupled to the Hitachi S-3400N scanning electron microscope. Samples were prepared as described for scanning electron microscopy (SEM), and the scanning electron microscope was operated using the same parameters as described for SEM.

Time-of-Flight Secondary Ion Mass Spectrometry. Time-of-flight secondary ion mass spectrometry (TOF-SIMs) was performed on areas of whole-mounted eye tissue that extended from the optic nerve head to the far periphery. Samples were dehydrated in a graded aqueous ethanol series (50%, 70%, 90% 100%, and 100%) and collected onto glass slides followed by chemical critical point drying with hexamethyldisilazane.

Time-of-flight secondary ion mass spectrometry was performed using a ToF.SIMS5 (IONTOF GmbH) equipped with a bismuth primary ion beam (Bi^{3+}) operating at 25 kV. To maximize the secondary ion yield from the biological samples, a Bi^{3+} cluster was used. The TOF-SIMs was also equipped with a low-energy electron flood gun for charge compensation. Before mass spectrometry, the sample surfaces were stripped of contaminants through bombardment with a 10 KeV Ar^{+} cluster ion beam (10 KeV Ar1000+). After removal of contaminants, the Bi^{3+} cluster was used to sputter secondary ions from the sample surface. Sputtered ions were passed through a time-of-flight mass analyzer, and the molecular fragment weight determined by the time it look to reach the detector. Mass spectrometry was performed over a range of 0 to 880 m/z (mass-to-charge ratio). Ions of interest included secondary molecular ions associated with calcium, phosphorus, calcium phosphates, and organic tissues such as amino acids.

Comparison with Clinical Imaging

Clinical retinal imaging data were available for donor 1. This consisted of central and midperipheral fundus color photography ($FF450^{plus}$; Carl Zeiss Meditec AG), central and midperipheral 55° near-infrared reflectance (NIR) imaging, spectral domain OCT imaging of the macula, and fundus autofluorescence imaging (all Spectralis HRA-OCT; Heidelberg Engineering). Using a specialized program, Autopana Giga version 4.4.4, fundus color photographs and NIR images were stitched together to create a montage image. These stitched images were used to visually compare clinical features with OsteoSense stained whole-mount tissues. Unfortunately, there was no ICGA available for this patient.

Results

In total, 6 eyes from 4 PXE donors (age at death: 69−85 years) and 1 comparison eye of an anonymous donor (age at death: 63 years) eye were obtained and analyzed. Pseudoxanthoma elasticum donors 1 and 2 had 2 pathogenic variants in the *Abcc6* gene; in donor 3, only 1 pathogenic variant was found, and donor 4 was not tested for pathogenic *Abcc6* variants but a first-degree relative had a confirmed genetic PXE diagnosis (variants can be found in Table S1). Pseudoxanthoma elasticum donors 3 and 4 both had a retinal phenotype including long angioid streaks that confirmed the PXE diagnosis.

Ophthalmological Manifestations

All 4 PXE donor eyes had end-stage retinal disease, including severe scarring, hyperpigmentation, and extensive atrophy, which were visible together with postmortem retinal damage on postmortem images (Fig S1). The visual acuity, if available, and details on clinical imaging are presented in Table S2 (available at www.ophthalmologyscience.org).

Clinical imaging comprising color fundus photography (Fig 2A), NIR (Fig 2B, C) and spectral-domain OCT (Fig 2D, E) revealed severe scarring and macular atrophy in donor 1. NIR (Fig 2C) shows the typical hyperreflective zone that likely represents BM calcification (Fig 2C, bordered by red dashed line). Furthermore, NIR revealed a distinct hyporeflective zone (Fig 2C, bordered by blue dashed line) with unknown clinical significance. The comparison eye had a normal retinal phenotype based on postmortem retinal imaging.

Hydroxyapatite Staining Characteristics

Osteosense staining of whole-mounted PXE eyes revealed extensive calcium phosphate precipitation (Fig 3A−D), which was visible as a meshwork-like pattern. A diffuse staining was also visible in the central and midperipheral regions of BM (Fig 3A−D). In contrast, in the comparison eye, precipitation of hydroxyapatite (HAP) was visible as snowflake-like deposits with a diameter of < 20 μm in the posterior pole (Fig 3E, F).

OsteoSense staining of cross sections obtained from PXE eyes revealed confluent calcium phosphate deposition (probably HAP) in the central BM. (Fig 3A, B; Fig S4, available at www.ophthalmologyscience.org). In contrast,

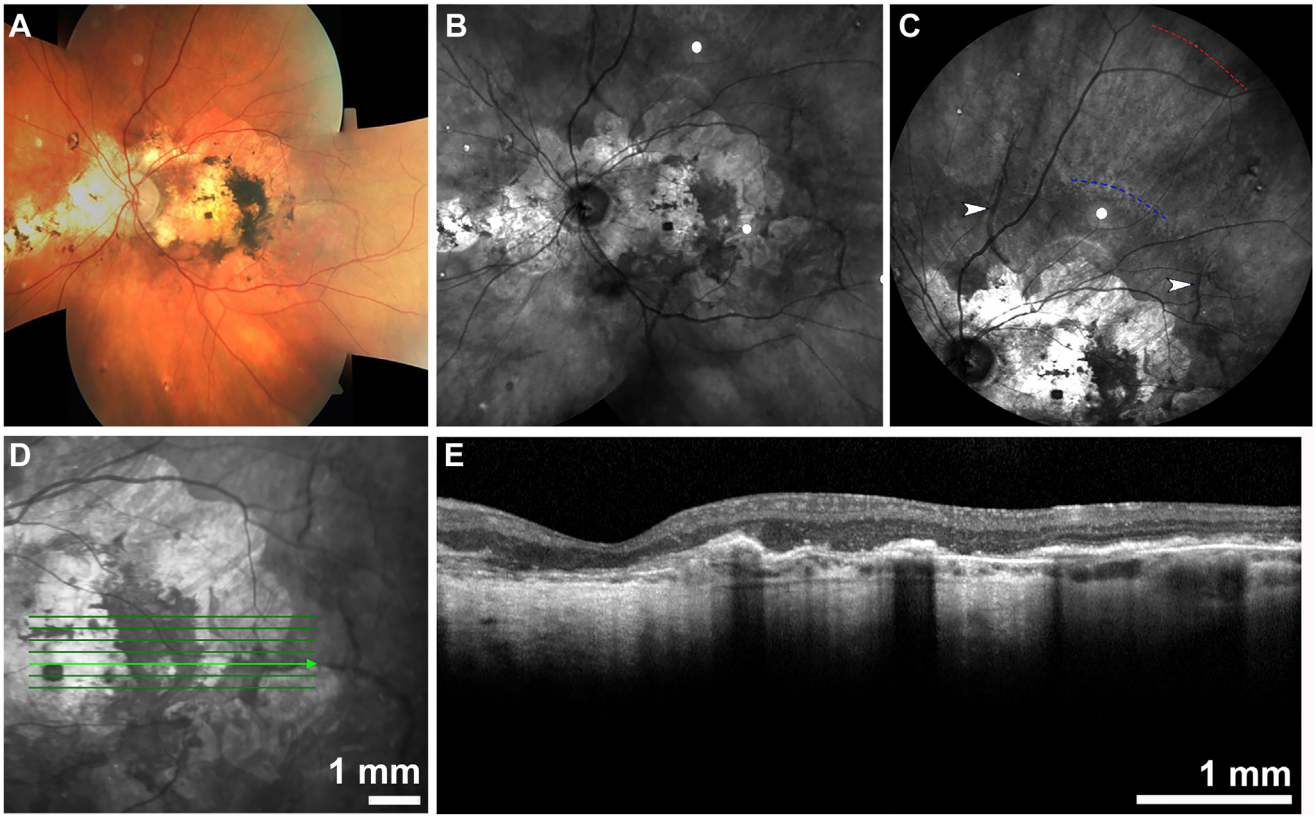

Figure 2. Clinical retinal imaging of donor 1 with pseudoxanthoma elasticum. **A,** Color fundus photography shows severe scarring and macular atrophy. **B, C,** Near-infrared reflectance imaging is superior in visualizing the characteristics of Bruch's membrane (BM) calcification. The red dashed line in panel (**C**) presumably represents a transition zone from a calcified BM to a normal fundus reflex. The blue dashed line (**C**) indicates a transition zone between a hypo- and a hyperreflective zone on near-infrared reflectance (NIR). The white arrowheads (**C**) indicate angioid streaks. **D,** NIR image showing a region of severe macular atrophy and scarring. **E,** OCT with the corresponding NIR image in panel (**D**). Note: the white dot in panels (**B**) and (**C**) is an artifact of the imaging modality.

calcium phosphate deposition in the peripheral BM was intermittent (Fig 5C, D). Interestingly, in the periphery, OsteoSense staining occurred preferentially in BM adjacent to the lumen of the choriocapillaris, as opposed to the pillars (Fig 5C, D).

Elemental Analysis

Scanning EM Coupled with Energy-Dispersive x-ray Spectroscopy. Scanning EM (SEM; Fig 6A, B) coupled with energy-dispersive x-ray spectroscopy (EDX; Fig 6C–F) confirmed the presence of calcium (Ca) and phosphorus (P) within regions of calcified BM in patients with PXE.

In PXE patients, x-ray emission peaks were identified at 2.01 keV, 3.37 keV, and 4.01 keV, which correspond to phosphorus KL3, calcium KL3 and calcium KM2 transitions. These peaks were absent in the control eye. Elemental mapping confirmed the enrichment of Ca (Fig 6D) and P (Fig 6F) within BM of PXE eyes compared with similar regions in the control eye (Fig 6C, E).

Time-of-Flight Secondary Ion Mass Spectrometry. Secondary molecular ions consistent with calcium phosphate, including molecular ion peaks at 39.99 m/z, 47.01 m/z, and 102.96 m/z that correspond, respectively, to [Ca+], [PO+], and [$CaPO_2$+] were readily identified on mass spectra obtained from BM of PXE eyes (Fig 7). Further analysis also identified several peaks separated by 55.9 m/z that correspond to a [CaO+] secondary molecular ion, which is a building block of HAP.[35] Importantly, mapping the sum of all identified peaks associated with HAP, including [Ca+], onto retinal cross sections, confirmed the localization of HAP to the BM (Fig 7A–C, arrow). In contrast, soft organic tissues were identified by mapping for the amino acid proline ([C_4H_8N+]; Fig 7D). Overlaying the secondary ion maps for HAP (Fig 5E, F, green hues) and proline (Fig 7E, F, orange/red hues) confirmed that HAP was restricted to BM. Accordingly, these data indicate that the BM calcification in PXE patients consists primarily of inorganic HAP.

Comparison with Clinical Imaging

To compare the distribution of calcification with clinical imaging features we compared the appearance of whole-mount samples with the clinical imaging of the same patient. We used landmark anatomical features such as the location of the optic nerve head, scarred tissue, and angioid streaks

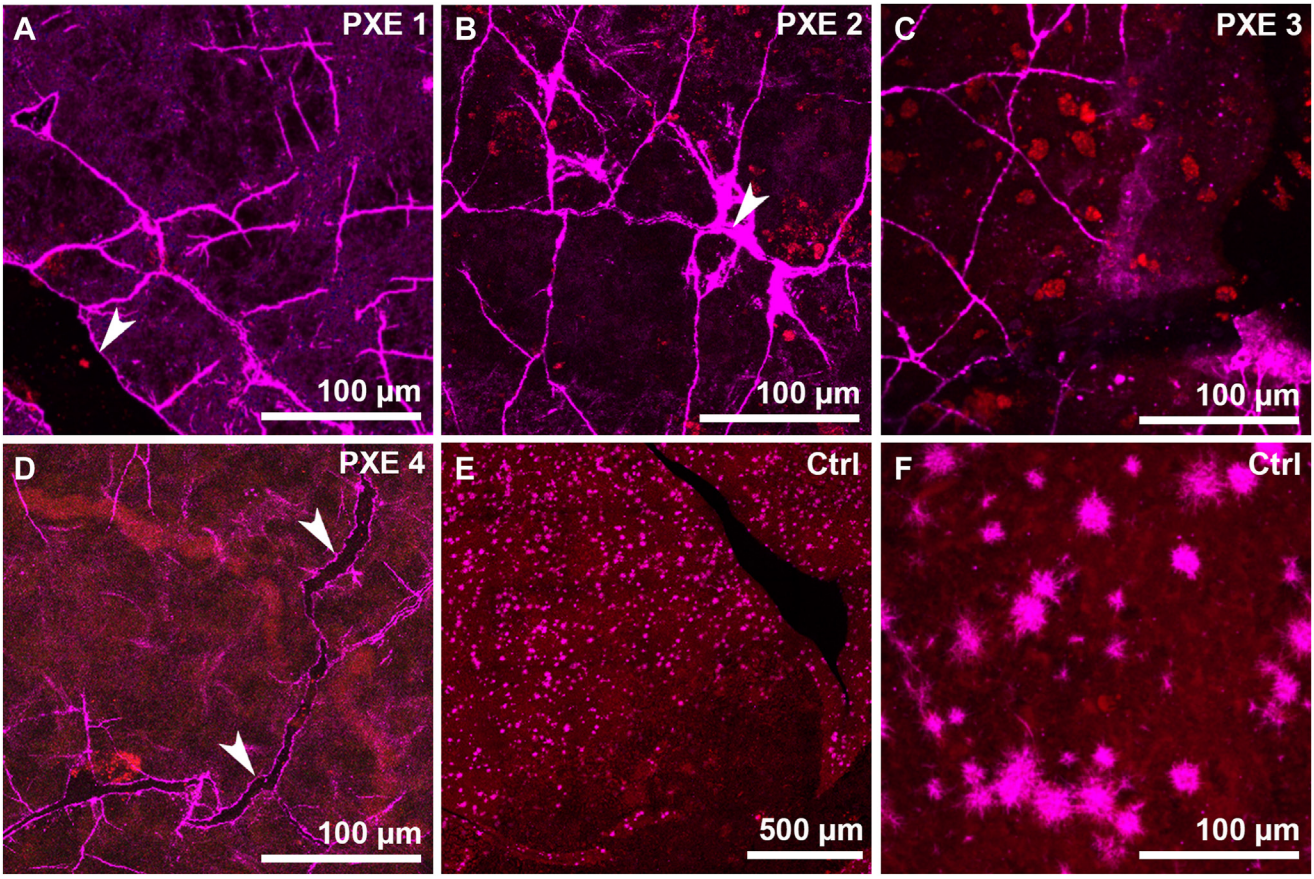

Figure 3. Representative images of Bruch's membrane calcification of human pseudoxanthoma elasticum (PXE) patient eyes (A–D) and a comparison donor eye (E, F). **A–D,** Osteosense staining of fixed tissues from eyes from PXE donors. The white arrows in (**A**), (**B**) and (**D**) indicate staining of hydroxyapatite along the edges of "cracks" within the meshwork. In (**A**), this likely represents an angioid streak. **E,** Osteosense staining of fixed tissue from a control donor with no reported underlying health conditions. **F,** A higher magnification of panel (**E**). OsteoSense staining in magenta; autofluorescent signal of Bruch's membrane in red. Images were obtained from *z*-stack maximal projections.

(Fig 8). Using these features, we located NIR hyperreflective and hyporeflective zones on postmortem tissues (red and blue dashed lines). After identifying specific features, we dissected a wedge from the macular area through to the far periphery for further analysis (Fig 9, dashed line box).

Elemental analysis reveals carbon, calcium, and phosphorus on the near surface of the tissue exposed to the electron beam (Fig 9B–D). Calcium and phosphorous were homogeneously detected on the surface of the midperipheral zone (Fig 9B–D, between red and blue dashed lines). In the periphery, the calcium and phosphorus signals were intermittent (Fig 9B–D, left of the red dashed line).

OsteoSense labeling corresponds with the elemental analysis from the blue line to the far periphery (Fig 9E). Figure 9E shows extensive neovascularization depicted by the AlexaFluor 568 labeling (Fig 9E, red) on the surface of BM.

SEM revealed 3 distinct calcified structures: a thin barbed wire-like structure (Fig 10B, C, F), fully calcified fibers (Fig 10C, D, G), and spherical structures (Fig 10E). In Figure 10C, there is a transition from the thin barbed wire-like structure to the fully calcified fibers. All of these contain calcium and phosphorous after elemental analysis. Figure 10F, G shows the distribution of calcification across the BM in the periphery and in the macula, respectively.

The same angioid streak is visible on the OsteoSense labeling (Fig 9E, white arrow) and the backscattered electron (Fig 10A, arrow), indicating a break in the dense calcium and phosphate precipitate. This angioid streak is also visible on the NIR imaging in Figure 8C.

Discussion

To our knowledge, this is the first detailed study examining the composition and distribution of BM calcification on clinical and postmortem images from the same patient with PXE. Based on this parallel examination, we found that the clinical appearance of PXE corresponds well with the detected differences in HAP deposition. The eyes with PXE showed HAP precipitation throughout the BM.

Calcification is a process that can occur as part of aging in many tissues, although excessive calcification is associated with pathological aging.[36] In the sub-RPE space in the

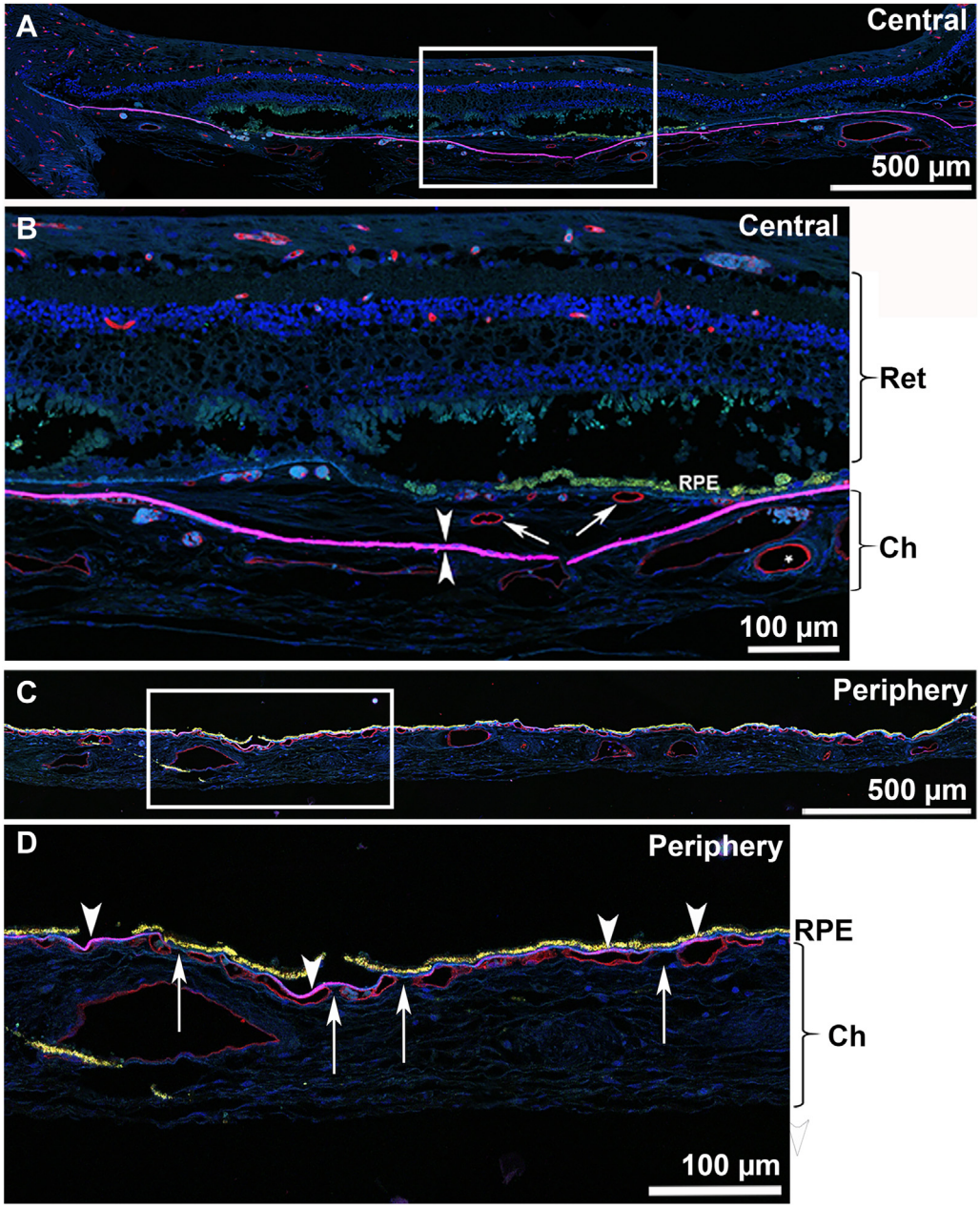

Figure 5. Hydroxyapatite-specific staining (Osteosense 680EX) of cross sections of an eye enucleated from a patient with pseudoxanthoma elasticum (donor 1). **A,** A low-magnification confocal image of the macular region. The white box indicates the region of interest shown in panel B. **B,** A high-magnification image of the macular region. OsteoSense staining (magenta) is extensive and confluent in the central macula Bruch's membrane (BM; indicated by compact white arrowheads). A region of choroidal neovascularization can also be observed between the retinal pigment epithelium (RPE) and calcified BM, as indicated by the presence of active blood vessels (white thin arrows). A crack in BM is also present. **C,** A low-magnification confocal image of the periphery. The white box indicates the region of interest shown in panel (**D**). **D,** Osteosense-positive regions (magenta; arrowheads), which indicate the presence of calcium phosphate, occur intermittently in the periphery. Deposition of calcium and phosphate seems to be localized to regions of BM above the vascular lumen (white arrowheads), whereas deposition appears to be limited above the vascular pillars in between the vascular lumen (white thin arrows). Blue, Hoechst 33342; Magenta, OsteoSense 680EX; red, biotinylated *Ulex europaeus* agglutinin-I-streptavidin Alexafluor 568.

eye, calcification appears in the form of calcified spherules, which seem to play an intrinsic role in sub-RPE deposit formation,[37–41] HAP nodules that are associated with the rapid progression to end-stage AMD,[39] and calcification of BM.[39] Pathological BM calcification is associated with breaks in the BM, the so-called angioid streaks. These disruptions of BM allow choroidal vessels to penetrate the subretinal space and thereby lead to choroidal neovascularization,[25] the main cause of vision loss in PXE.[42]

The process and the variability of BM calcification in PXE is, however, not fully understood. Because PXE is defined as calcification of elastin fibers in the skin,[43] it was

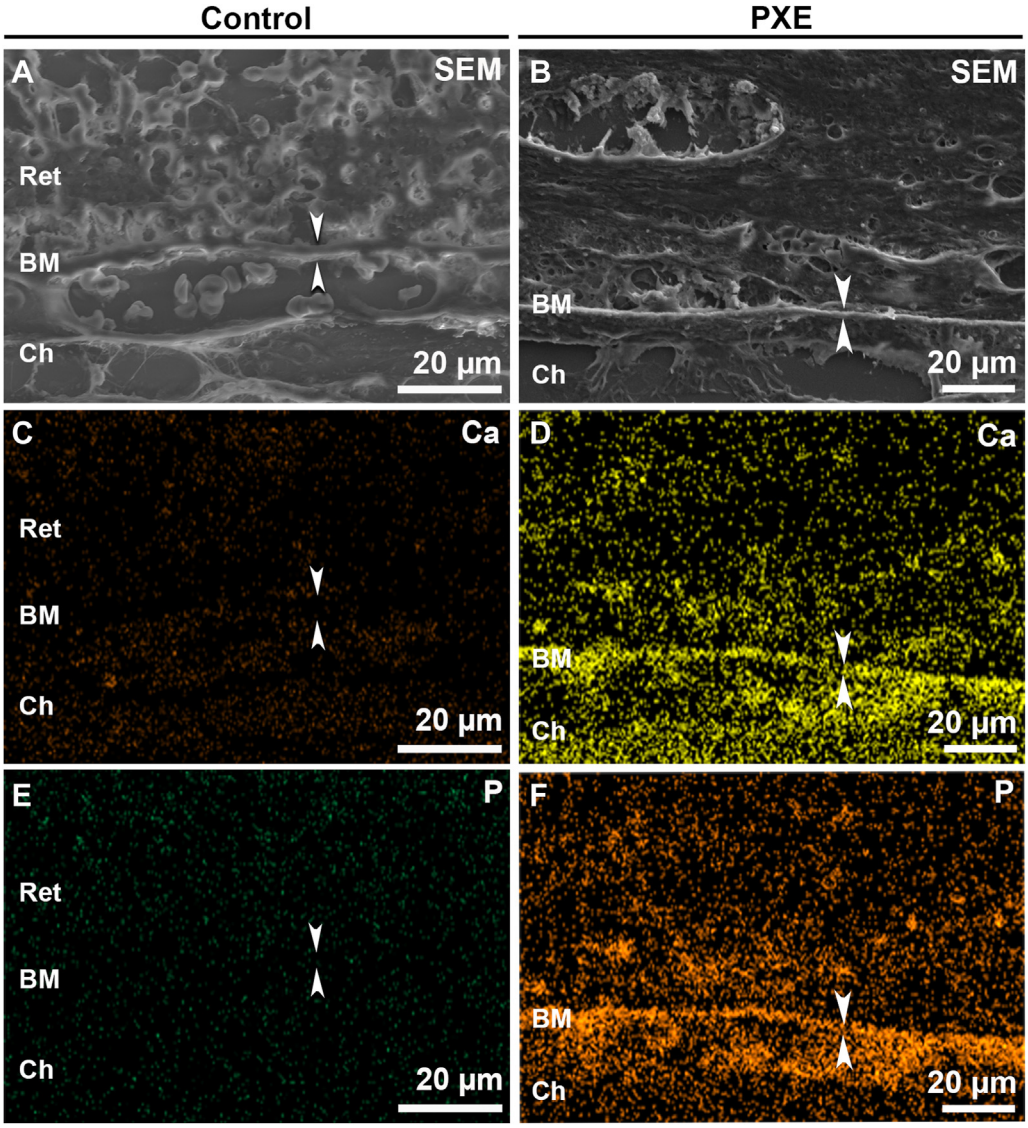

Figure 6. Scanning electron microscopy coupled with energy-dispersive x-ray spectroscopy (SEM-EDX) of Bruch's membrane (BM) in control and pseudoxanthoma elasticum (PXE) eyes. **A,** A backscattered electron micrograph of a cross section the retina–choroid complex in a healthy control eye. **B,** A backscattered electron micrograph of the retina–choroid complex of an eye enucleated from a patient with pseudoxanthoma elasticum. Note that BM appears brighter (white hues) in panel (**B**) compared with panel (**A**), suggesting that BM is composed of elements of higher atomic weight in this sample. **C,** An elemental map showing the distribution of calcium in BM of a control eye. **D,** An elemental map showing the enrichment of calcium in BM of PXE eyes. **E,** An elemental map showing the distribution of phosphorus in BM of a control eye. **F,** An elemental map showing the enrichment of phosphorus in BM of PXE eyes. Arrowheads delimit the BM. Ca = calcium; Ch = choroid; P = phosphorus; Ret = retina; RPE = retinal pigment epithelium; SEM = scanning electron microscopy.

suggested that the calcification of the elastic layer in the BM underpins the clinical phenotype of peau d'orange and angioid streaks.[44–46] Chong et al[47] found a decreased thickness and increased fragmentation of the elastic layer in BM with age in the macular area of unaffected eyes, which could support the hypothesis that underlying topographical differences of elastin fibers predispose pathological calcification in PXE.[28] However, calcification of the collagen layers in the BM had also been suggested in previous observations using transmission electron microscopy in humans and in an animal model.[48,49] Indeed, we found that in addition to the elastic fibers, both the inner and outer collagenous layers of the BM also undergo extensive mineralization (Fig 10). Therefore, it appears that in the eye, calcification of all 3 fibrous layers of the BM contributes to calcification in PXE. Our detailed multimodal analysis also confirmed that the calcification is in the form of calcium phosphate (including HAP) precipitation onto the fiber surfaces.

The proof of the extensive rigidity was the meshwork-like pattern of HAP labeling on whole-mount images (Fig 3A–D). We hypothesize that this was a consequence of

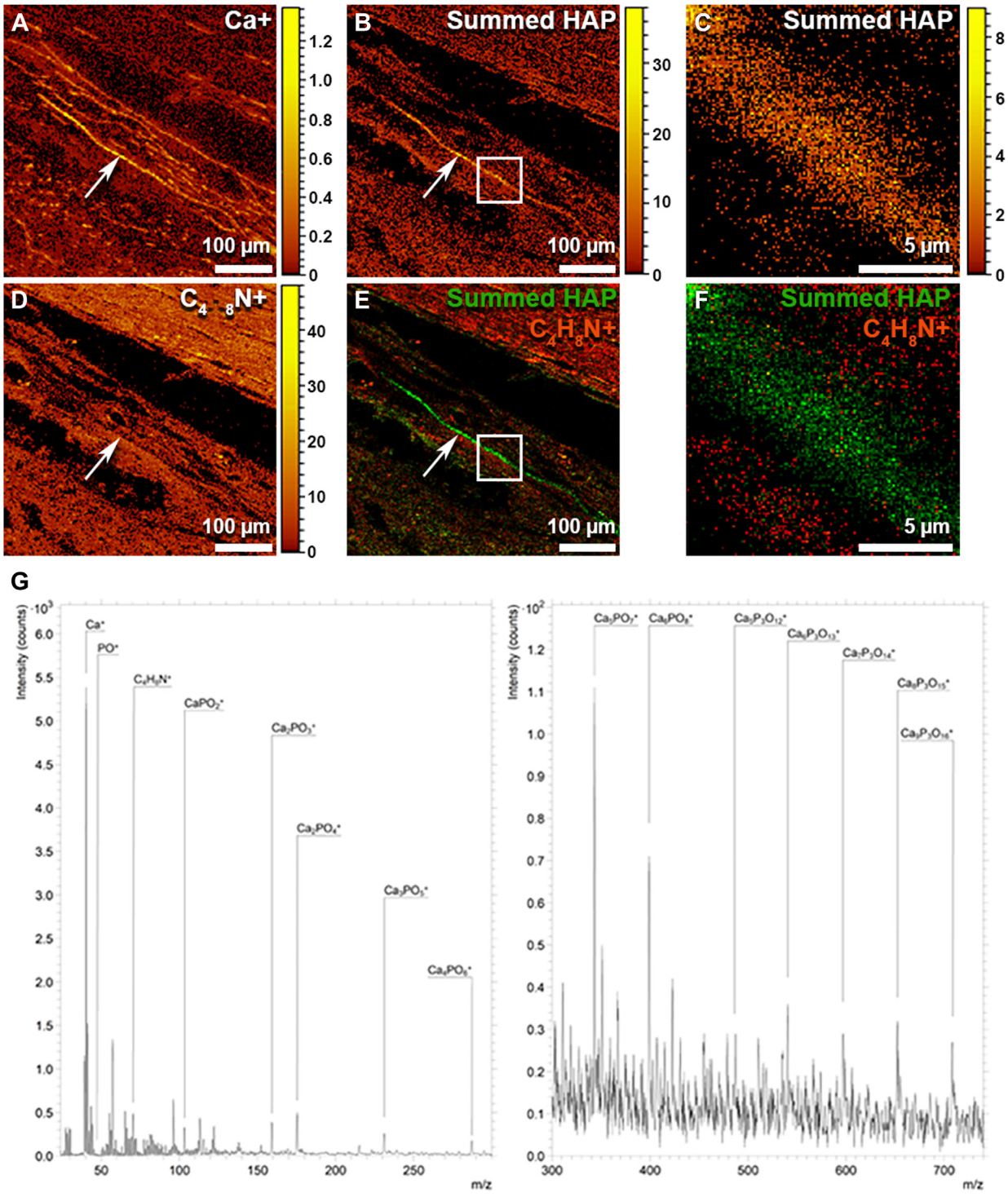

Figure 7. Time-of-flight secondary ion mass spectrometry indicates that calcification of Bruch's membrane of patients with pseudoxanthoma elasticum (PXE) is formed from inorganic hydroxyapatite (HAP). **A,** Secondary molecular ion map showing the localization of molecular ions characteristic of calcium (Ca+). **B,** A secondary ion map showing the localization of fragment molecular ions associated with HAP. **C,** A higher-magnification image showing the region highlighted by the white square in panel B. **D,** A secondary ion map of proline (C_4H_8N+) indicating areas of soft organic tissue. **E,** A secondary ion map showing that fragment ions associated with HAP (green) are localized to the Bruch's membrane in eyes from patients with PXE, whereas the surrounding tissues are composed of organic material (red/orange hues). **F,** A higher magnification of the region indicated by the white square in panel (**E**). **G,** A secondary ion mass spectrum (divided into 2 panels with differing sensitivity for low and high mass ranges) showing numerous calcium phosphate fragment ions separated by 55 m/z, which corresponds to a CaO molecule. These peaks, when observed together, are highly indicative of HAP.

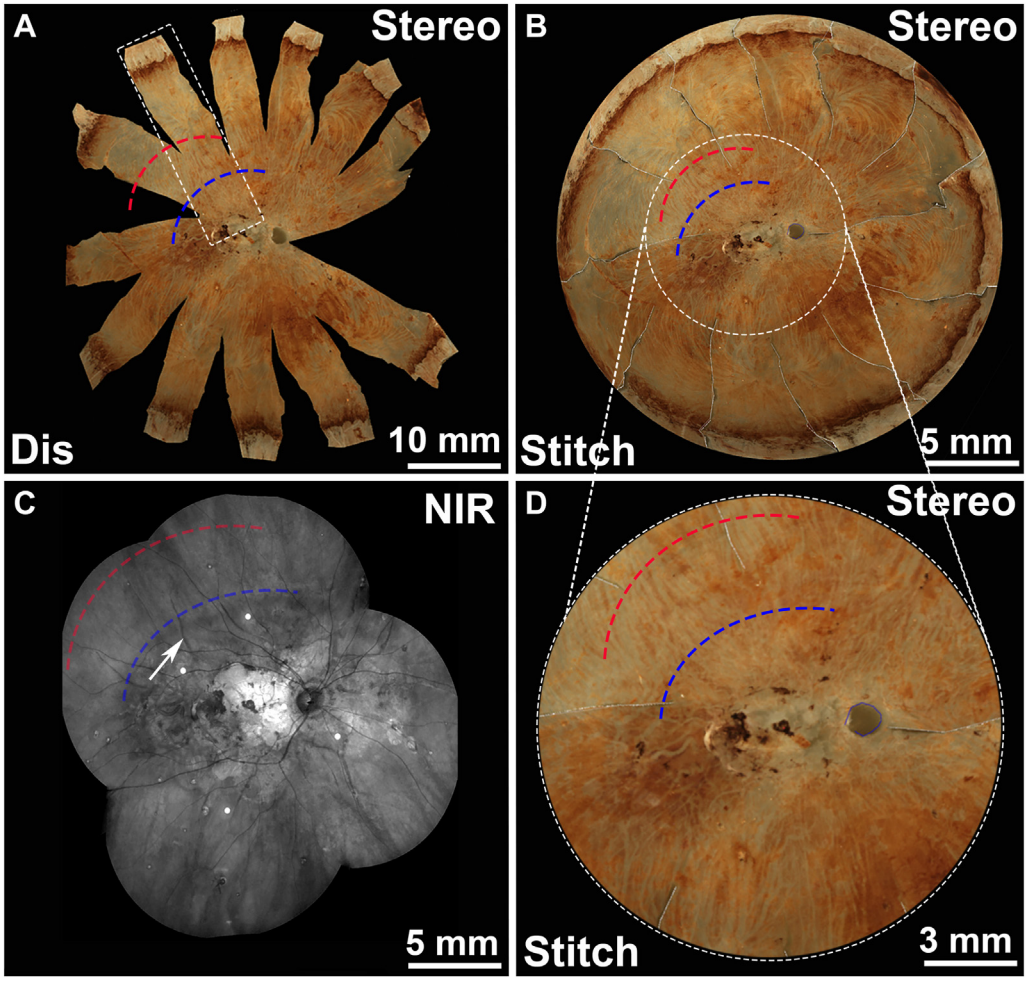

Figure 8. A comparison of clinical features using postmortem imaging and corresponding clinical fundus imaging of a pseudoxanthoma elasticum (PXE) donor eye (patient 1). **A,** Whole-mounted and dissected PXE eye in which the neural retina has been removed. **B,** Postimage processing (stitching) of the dissected tissue shown in panel (**A**). **C,** A stitched 55° near-infrared reflectance (NIR) clinical image that corresponds to the postmortem tissue shown in panels (**A**, **B**, **D**). **D,** High-magnification image of the postmortem tissue shown in panel (**B**). This region corresponds to the NIR image shown in panel (**C**). The blue dashed line indicates the transition zone between NIR hyporeflectivity and NIR hyperreflectivity. The red dashed line indicates a transition zone between NIR hyperreflectivity and NIR isoreflectivity. The white arrow in (**C**) indicates an angioid streak. Scale bars: A and B, 20 mm; C and D, 10 mm. Dis = dissected; Stereo = stereo dissection microscope image.

the mechanical stress caused by flattening the eye to prepare the whole-mount PXE tissues. This stress resulted in "cracking" of the calcified BM. The "fresh" mechanical break allowed direct exposure of HAP to OsteoSense labeling, hence the cracked appearance. Interestingly, "old" breaks (angioid streaks) were not labeled as intensely (Fig 3A). The most likely explanation for the relatively reduced labeling between the "fresh" breaks is that HAP is known to bind various proteins and lipids.[37] Thus, accumulating organic material on the surfaces of HAP[50,51] may have prevented the binding of OsteoSense to HAP (Fig 3). Further evidence for this explanation was obtained by labeling of sections of whole eyes that showed continuous intense labeling in the posterior pole across the full thickness of the BM (Fig 5). Fluorescent dyes used to label chorioretinal calcification might have potential as clinical imaging biomarkers, because they might aid in the early detection and monitoring of BM calcification in vivo.[52]

Calcification in the peripheral areas was intermittent, and HAP precipitation often appeared above the vascular lumen of the choriocapillaris (Fig 5C, D; Fig S4). In contrast, calcified spherules in drusen are associated with choriocapillary pillars.[38,53] This suggests that the calcification process of BM might differ from drusen calcification. We propose that BM calcification might be linked with the availability of circulating calcium and phosphate, and possibly pyrophosphate,[54] and the distinctly different microenvironment in the 3-layer BM, rather than the problem of clearance, as suggested for sub-RPE deposit formation.[4,5,7] This aligns with the hypothesis that PXE is a metabolic disease and HAP precipitation is systemically induced.[55] The choriocapillaris is different across the various regions

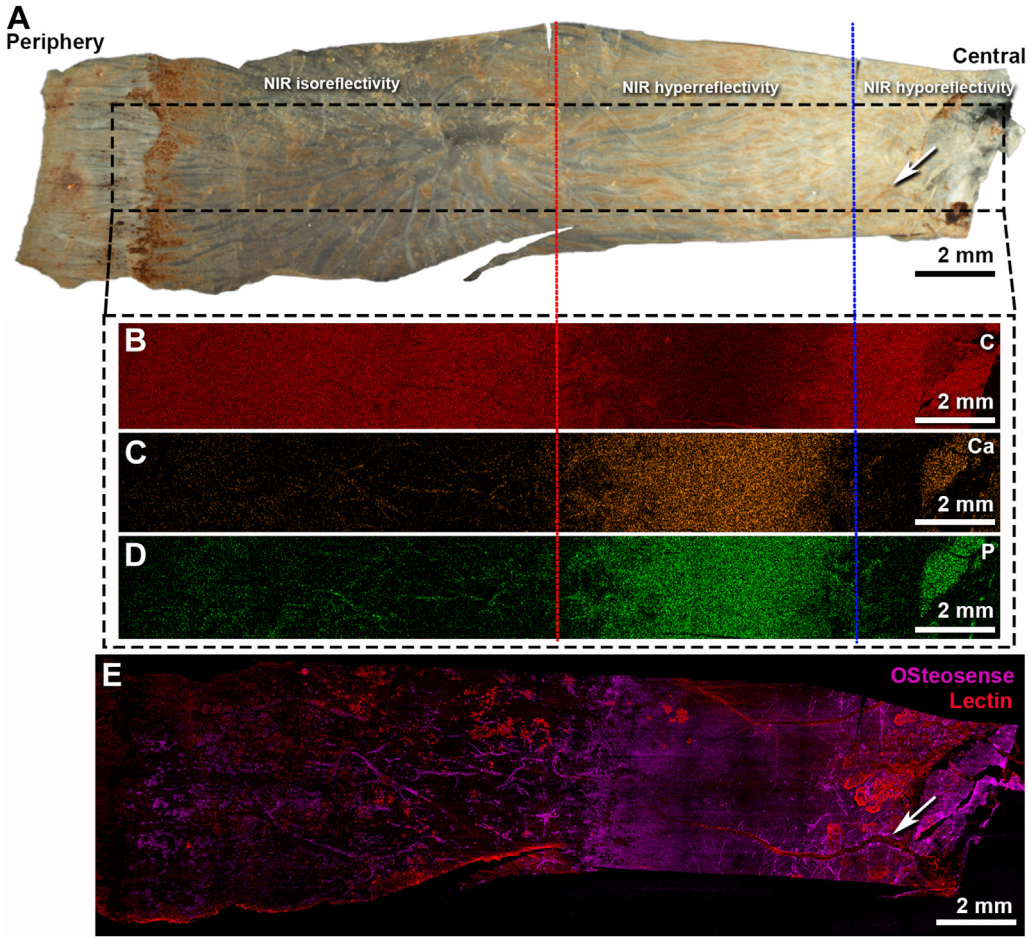

Figure 9. The topographical distribution and characteristics of hydroxyapatite precipitation in Bruch's membrane (BM) in a pseudoxanthoma elasticum (PXE) donor eye (patient 1). **A,** A light microscopy image showing a whole-mounted BM–Choroid complex from a PXE patient. This was obtained using a stereo dissection microscope. This region corresponds to the tissue indicated in the white dashed box in Figure 6A. **B–D**, Elemental maps confirmed changes in CaP distribution across the central–peripheral axis. The tissue shown in (**B–D**) corresponds to that indicated within the white dashed box in (**A**)**. E,** Hydroxyapatite-specific staining (OsteoSense 680EX) of the corresponding whole-mounted tissue. The white arrows in (**E**), indicates a single angioid streak (visible on Fig 6C). The red and blue dashed lines correspond to those in Figure 6. The blue line indicates the transition zone between near-infrared reflectance (NIR) hyporeflectivity and NIR hyperreflectivity. The red dashed line indicates a transition zone between NIR hyperreflectivity and NIR isoreflectivity.

across the eye.[56] In the posterior pole, the choriocapillaris forms a dense, honeycomb-like structure with shorter intercapillary distances and a higher frequency of endothelial fenestrations compared with the peripheral choriocapillaris.[57–61] These properties may explain the dense and continuous calcification of the fibers in BM in the posterior pole and the less confluent calcification toward the retinal periphery. This raises the hypothesis that modifying the availability of calcification regulators in the peripheral circulation could reduce the progression of BM calcification in PXE.[62–64]

The calcification changes on postmortem tissues seem to correspond with the clinical features on NIR clinical images. Confluent NIR hyperreflectivity, clinically also regarded as "coquille dóeuf,"[65] corresponds to fully calcified BM, whereas the area between the hyperreflective and isoreflective zones on NIR imaging corresponds to a transition from a fully calcified BM to intermittent calcification (Figs 8, 10C, red dashed line). The most central zone, which is NIR hyporeflective, corresponds with the meshwork-like OsteoSense labeling and increased carbon signal (Fig 9, right of the blue dashed line). As discussed above, this might be caused by an accumulation of organic material. We clinically observed that the topographical distribution of NIR hyporeflectivity roughly corresponds with the zone of ICGA hypofluorescence (unpublished work, Fig S11, available at www.ophthalmologyscience.org). Interestingly, the ICGA hypofluorescence observed in PXE patients shares a similar appearance with age-related scattered hypofluorescent spots on late-phase ICGA, which are thought to be associated with lipid accumulation in BM.[66,67] Perhaps, the buildup of organic material directly or indirectly reduces the ICG uptake by RPE cells and thereby causes the typical hypofluorescence in the ICGA late phase, but this hypothesis will need further investigation.

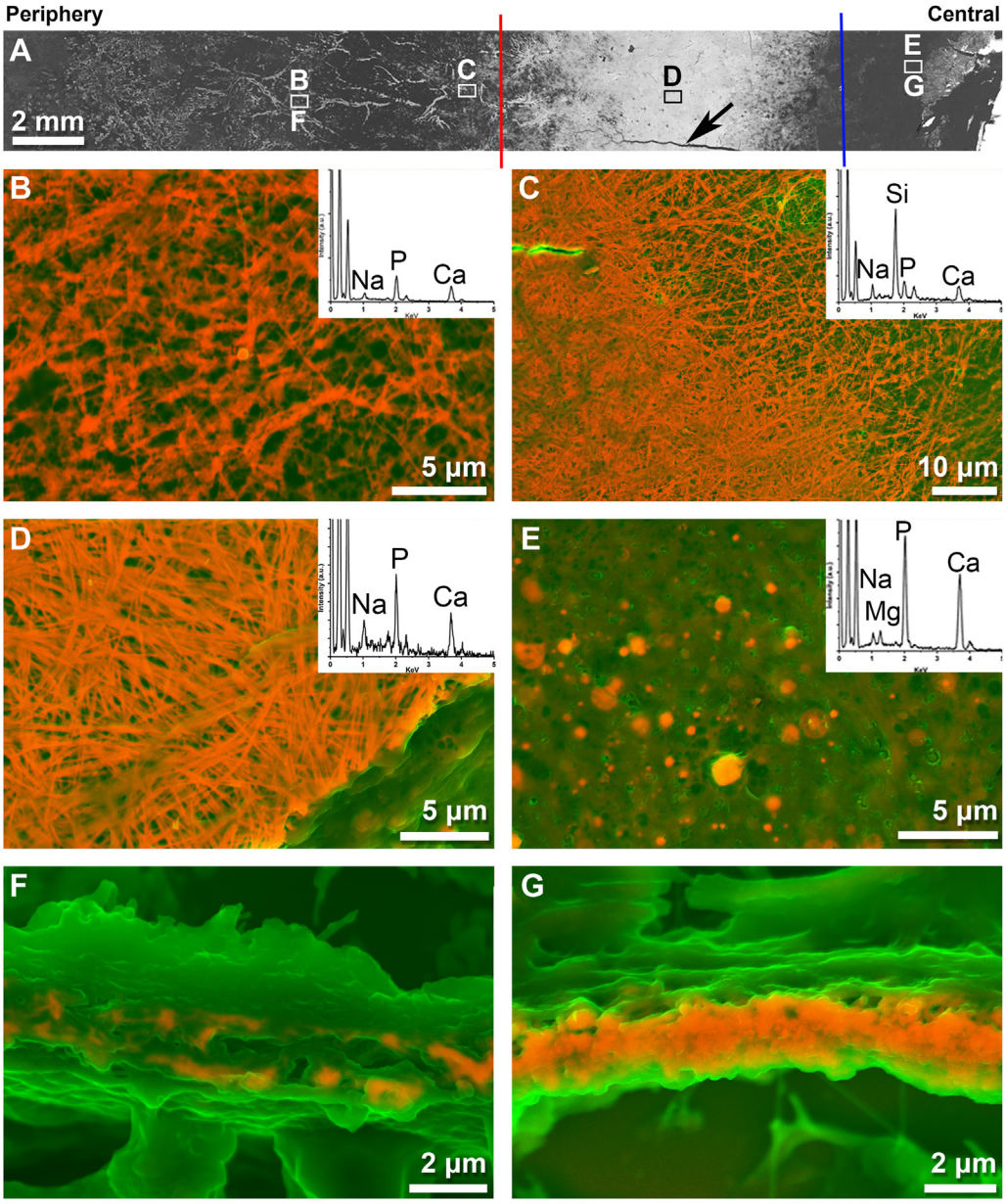

Figure 10. Density-Dependent Color Scanning Electron Microscopy (DDC-SEM) of Bruch's membrane (BM) calcification in a pseudoxanthoma elasticum (PXE) donor eye (patient 1). **A,** A backscattered electron micrograph showing compositional differences across the central peripheral axis. This region corresponds to the area indicated within the white dash boxed in Figure 7. Brighter hues correspond to regions composed of higher atomic weight elements. The black arrow indicates an angioid streak. **B**–**E**, DDC-SEM micrographs at different regions across the central peripheral axis. Panels correspond to the letters associated with the small boxes shown in panel **(A)**. Calcium phosphate is presented in orange and organic material in green. Insets in each panel are the representative energy-dispersive x-ray spectroscopy spectra for the calcification. **F, G,** Cross sections of BM corresponding with the white boxes in panel **(A). F,** Calcium phosphate deposition in the inner and outer aspects of BM in the periphery. **G,** Calcium phosphate throughout all fibrous layers of BM in the macula.

In the retinal periphery, we observed scattered HAP precipitation, although this did not correspond to an increased fundus reflex nor NIR hyperreflectivity on clinical imaging. However, it is important to point out that these areas were not imaged extensively in our study, but previous studies using widefield imaging of PXE did not show an increased reflex in the peripheral retina either.[65,68]

Previous clinical imaging studies suggested the existence of a so-called temporal sparing, which is the phenomenon of nonconfluent BM calcification in the temporal region in eyes with PXE.[27,28] This was not detectable on NIR imaging in our study, probably due to extensive scarring. Nevertheless, our findings may provide further insight into this phenomenon; we found that HAP precipitation was

often found above the vascular lumen of the choriocapillaris; therefore, BM calcification could (partly) be dependent on the flow through the choriocapillary vessels. The choriocapillary perfusion is lower in the temporal area than in other areas of the central and midperipheral area.[69] Perhaps, a reduced choriocapillary flow in the temporal region explains the phenomenon of temporal sparing in PXE.

This study has several strengths. First, we were fortunate to obtain 6 eyes from 4 patients from donors with such a rare disease. This allowed the comparison of eyes of the same person with 2 approaches: examining changes on whole-mount tissues as well as on whole-eye sections. Second, we assembled a multidisciplinary team to study PXE using state-of-the-art analytical chemistry and molecular techniques to allow a detailed and unique inquiry into the pathological changes of the tissues. Third, for 1 of the eyes, we had access to clinical imaging taken before the eyes were donated for research after death. This allowed direct comparison between clinical and postmortem retinal imaging.

This study also has limitations. Not all donor samples had clinical imaging available. All donor eyes had end-stage retinal disease; therefore, it is difficult to distinguish what findings are part of the pathophysiological course of ectopic calcification and what findings were secondary to advanced BM calcification. In addition, the time of death to preservation was rather long or unknown in our donors that could have increased acidification in our samples.[70] This could have resulted in underestimating the level of calcification in vivo.[71] However, we believe this would not impact our conclusion.

In summary, this study confirmed that BM calcification in PXE consists of HAP and reveals involvement of both the elastic and the collagen layers of BM. We compared clinical imaging with postmortem analysis which provides insight into the structural alterations of clinically visible abnormalities. Mild BM calcification in normal aging might share $\geq$ 1 underlying mechanisms with PXE, although further research is warranted to confirm this.

Acknowledgments

The TOF-SIMS analysis was funded by the Engineering and Physical Sciences Research Council, UK (Grant EP/H006060/1) and by the Natural Environment Research Council, UK (Grant NE/J013382/1). The authors would like to thank the patients and their relatives who agreed to donate tissue for research. The tissue for this project was provided by the Dutch National Expertise Center of PXE, the Netherlands Institute for Neuroscience, the University College London Institute of Ophthalmology and Moorfields Eye Hospital Eye Tissue Repository supported by National Institute for Health Research funding. Imre Lengyel is a member of the International Network on Ectopic Calcification (INTEC, www.itnintec.com)

Footnotes and Disclosures

Originally received: May 3, 2023.
Final revision: October 10, 2023.
Accepted: October 18, 2023.
Available online: October 24, 2023. Manuscript no. XOPS-D-23-00091R2.

[1] Department of Ophthalmology, University Medical Center Utrecht, Utrecht University, The Netherlands.

[2] Wellcome-Wolfson Institute for Experimental Medicine, School of Medicine, Dentistry and Biomedical Science, Queen's University Belfast, Belfast, Northern Ireland, United Kingdom.

[3] Department of Medical Physics and Biomedical Engineering, University College London, London, United Kingdom.

[4] Department of Materials, Imperial College London, London, United Kingdom.

[5] Departments of Human Genetics and Ophthalmology, Amsterdam UMC, location AMC Academic Medical Center, University of Amsterdam, Amsterdam, The Netherlands.

[6] Emma Center for Personalized Medicine, Amsterdam UMC, University of Amsterdam, The Netherlands.

[7] Roche Pharma Research and Early Development, Roche Innovation Center Basel, Basel, Switzerland.

[8] University of Maryland School of Medicine, Department of Biochemistry and Molecular Biology, Baltimore, Maryland.

[9] Department of Vascular Medicine, University Medical Center Utrecht, Utrecht University, The Netherlands.

*S.R. and M.G.P. contributed equally to this work.

Disclosure(s):

All authors have completed and submitted the ICMJE disclosures form.

The authors have made the following disclosures: M.G.P.: Research support − F. Hoffmann LaRoche Ltd; Travel support − Queen's University Belfast.

C.N.B.: Research support − Department for the Economy.

R.B.T.: Grant − NIH National Eye Institute; Principal − Pokegama Technologies, Inc.

E.K.: Employment − Hoffman LaRoche.

R.v.L.: Advisory board − EPICAT study (Effectiveness of periocular drug injection in Cataract surgery).

I.L.: Unrestricted support − Hoffman LaRoche, Optos Plc; Patent − Methods and compositions for detecting drusen and predicting age-related macular degeneration Patent number: 9801955.

The other authors have no proprietary or commercial interest in any materials discussed in this article.

Supported by Rotterdamse Stichting Blindenbelangen, Stichting Vrienden UMC Utrecht, Donders-Binkhorststichting, Fischer Stichting, Stichting tot verbetering van het Lot der Blinden, Stichting PXE Fonds (S.R.); National Eye Institute, EY 030443, NIH (RBT); Unrestricted grant (I.L.) and a postdoctoral fellowship (M.P.) from Hoffman LaRoche. Fight for Sight UK (S.B. and I.L.). I.L. and R.T. are supported by the grant "Ectopic soft tissue calcification (NIH-P01 AG081167). The funding organizations had no role in design or conduct of this research.

Parts of this research were presented at the ARVO annual meeting, May 1−4, 2022, Denver, CO; the Dutch Ophthalmological Society annual meeting, June 29−July 1 2022, Groningen, The Netherlands; and the ARVO annual meeting, April 23−27 2023, New Orleans, LA.

HUMAN SUBJECTS: Human subjects were included in this study. This study adhered to the tenets of the Declaration of Helsinki and the work on the cadavers was approved by the research ethics committee of the faculty of Medicine, Health and Life Sciences of Queens University Belfast. Written informed consent for the use of the eye tissue was obtained in each case.

No animal subjects were used in this study.

Author Contributions:

Conception and design: Risseeuw, Lengyel

Data collection: Risseeuw, Pilgrim, Bertazzo, Brown, Csincsik, Fearn, Bergen, ten Brink, Ossewaarde−van Norel, van Leeuwen, Lengyel

Analysis and interpretation: Risseeuw, Pilgrim, Bertazzo, Brown, Csincsik, Fearn, Thompson, Bergen, ten Brink, Kortvely, Spiering, Ossewaarde−van Norel, van Leeuwen, Lengyel

Obtained funding: Lengyel, Thompson, Rissieeuw

Overall responsibility: Risseeuw, Ossewaarde−van Norel, van Leeuwen, Lengyel

Abbreviations and Acronyms:
AMD = age-related macular degeneration; **BM** = Bruch's membrane; **EDX** = energy-dispersive x-ray spectroscopy; **HAP** = hydroxyapatite; **ICG** = indocyanine green; **ICGA** = indocyanine green angiography; **NIR** = near-infrared reflectance; **PXE** = pseudoxanthoma elasticum; **RPE** = retinal pigment epithelium; **SEM** = scanning electron microscopy; **TOF-SIMs** = time-of-flight secondary ion mass spectrometry.

Keywords:
Bruch's membrane, Calcification, Hydroxyapatite, Pseudoxanthoma elasticum.

Correspondence:
Imre Lengyel, The Wellcome-Wolfson Institute for Experimental Medicine, School of Medicine, Dentistry and Biomedical Science, Queen's University Belfast, 97 Lisburn Road, Belfast, BT9 7BL, UK E-mail: i.lengyel@qub.ac.uk.

References

1. Bergen AA, Plomp AS, Schuurman EJ, et al. Mutations in ABCC6 cause pseudoxanthoma elasticum. *Nat Genet*. 2000;25:228−231. https://doi.org/10.1038/76109.
2. Le Saux O, Urban Z, Tschuch C, et al. Mutations in a gene encoding an ABC transporter cause pseudoxanthoma elasticum. *Nat Genet*. 2000;25:223−227. https://doi.org/10.1038/76102.
3. Ramrattan RS, Van der Schaft TL, Mooy CM, et al. Morphometric analysis of Bruch's membrane, the choriocapillaris, and the choroid in aging. *Invest Ophthalmol Vis Sci*. 1994;35:2857−2864.
4. Sarks SH. Ageing and degeneration in the macular region: a clinico-pathological study. *Br J Ophthalmol*. 1976;60:324−341.
5. Sarks SH. Council Lecture. Drusen and their relationship to senile macular degeneration. *Aust J Ophthalmol*. 1980;8:117−130. https://doi.org/10.1111/j.1442-9071.1980.tb01670.x.
6. Gass JDM. *Stereoscopic Atlas of Macular Diseases: Diagnosis and Treatment*. 4th ed. Mosby; 1997.
7. Quinn N, Csincsik L, Flynn E, et al. The clinical relevance of visualising the peripheral retina. *Prog Retin Eye Res*. 2019;68:83−109. https://doi.org/10.1016/j.preteyeres.2018.10.001.
8. Hogan MJ, Alvarado J. Studies on the human macula. IV. Aging changes in Bruch's membrane. *Arch Ophthalmol*. 1967;77:410−420. https://doi.org/10.1001/archopht.1967.00980020412022.
9. Curcio CA, Johnson M. Structure, function, and pathology of Bruch's membrane. In: Ryan SJ, Schachat AP, Wilkinson DR, et al., eds. *Retina*. Elsevier; 2013:466−481.
10. Booij JC, Baas DC, Beisekeeva J, et al. The dynamic nature of Bruch's membrane. *Prog Retin Eye Res*. 2010;29:1−18. https://doi.org/10.1016/j.preteyeres.2009.08.003.
11. Guymer R, Luthert P, Bird AC. Changes in Bruch's membrane and related structures with age. *Prog Retin Eye Res*. 1999;18:59−90. https://doi.org/10.1016/B978-0-323-02598-0.50065-3.
12. Glenn JV, Mahaffy H, Wu K, et al. Advanced glycation end product (AGE) accumulation on Bruch's membrane: Links to age-related RPE dysfunction. *Invest Ophthalmol Vis Sci*. 2009;50:441−451.
13. Newsome DA, Huh W, Green WR. Bruch's membrane age-related changes vary by region. *Curr Eye Res*. 1987;6:1211−1221.
14. van der Schaft TL, Mooy CM, de Bruijn WC, et al. Histologic features of the early stages of age-related macular degeneration: a statistical analysis. *Ophthalmology*. 1992;99:278−286. https://doi.org/10.1016/S0161-6420(92)31982-7.
15. Sheraidah G, Steinmetz R, Maguire J, et al. Correlation between lipids extracted from Bruch's membrane and age. *Ophthalmology*. 1993;100:47−51. https://doi.org/10.1016/S0161-6420(13)31712-6.
16. Moore DJ, Hussain AA, Marshall J. Age-related variation in the hydraulic conductivity of Bruch's membrane. *Invest Ophthalmol Vis Sci*. 1995;36:1290−1297.
17. Starita C, Hussain AA, Patmore A, Marshall J. Localization of the site of major resistance to fluid transport in Bruch's membrane. *Invest Ophthlmol Vis Sci*. 1997;38:762−767.
18. Moore DJ, Clover GM. The effect of age on the macromolecular permeability of human Bruch's membrane. *Invest Ophthalmol Vis Sci*. 2001;42:2970−2975.
19. Hussain AA, Starita C, Hodgetts A, Marshall J. Macromolecular diffusion characteristics of ageing human Bruch's membrane: implications for age-related macular degeneration (AMD). *Exp Eye Res*. 2010;90:703−710. https://doi.org/10.1016/j.exer.2010.02.013.
20. Ethier CR, Johnson M, Ruberti J. Ocular biomechanics and biotransport. *Annu Rev Biomed Eng*. 2004;6:249−273. https://doi.org/10.1146/annurev.bioeng.6.040803.140055.
21. Bhutto I, Lutty G. Understanding age-related macular degeneration (AMD): Relationships between the photoreceptor/retinal pigment epithelium/Bruch's membrane/choriocapillaris complex. *Mol Aspects Med*. 2012;33:295−317.
22. Bourne RRA, Jonas JB, Flaxman SR, et al. Prevalence and causes of vision loss in high-income countries and in Eastern and Central Europe: 1990-2010. *The Br J Ophthalmol*. 2014;98:629−638. https://doi.org/10.1136/bjophthalmol-2013-304033.
23. Curcio CA, Johnson M, Rudolf M, Huang JD. The oil spill in ageing Bruch membrane. *Br J Ophthalmol*. 2011;95:1638−1645. https://doi.org/10.1136/bjophthalmol-2011-300344.
24. Klein R, Klein BEK, Tomany SC, et al. Ten-year incidence and progression of age-related maculopathy: the Beaver Dam eye study. *Ophthalmology*. 2002;109:1767−1779.
25. Spraul CW, Lang GE, Grossniklaus HE, Lang GK. Histologic and morphometric analysis of the choroid, Bruch's membrane, and retinal pigment epithelium in postmortem eyes with age-related macular degeneration and histologic examination of surgically excised choroidal neovascular membranes. *Surv Ophthalmol*. 1999;44:10−32. https://doi.org/10.1016/S0039-6257(99)00086-7.
26. Jansen RS, Kucukosmanoglu A, de Haas M, et al. ABCC6 prevents ectopic mineralization seen in pseudoxanthoma elasticum by inducing cellular nucleotide release. *Proc Natl*

Acad Sci U S A. 2013;110:20206–20211. https://doi.org/10.1073/pnas.1319582110.
27. Charbel Issa P, Finger RP, Gotting C, et al. Centrifugal fundus abnormalities in pseudoxanthoma elasticum. *Ophthalmology*. 2010;117:1406–1414. https://doi.org/10.1016/j.ophtha.2009.11.008.
28. Risseeuw S, van Leeuwen R, Imhof SM, et al. The natural history of Bruch's membrane calcification in pseudoxanthoma elasticum. *Ophthalmol Sci*. 2021;1:100001. https://doi.org/10.1016/j.xops.2020.100001.
29. Charbel Issa P, Finger RP, Holz FG, Scholl HPN. Multimodal imaging including spectral domain OCT and confocal near infrared reflectance for characterization of outer retinal pathology in pseudoxanthoma elasticum. *Invest Ophthalmol Vis Sci*. 2009;50:5913–5918. https://doi.org/10.1167/iovs.09-3541.
30. Hagedoorn A. Angioid streaks and traumatic ruptures of Bruch's membrane. *Br J Ophthalmol*. 1975;59:267.
31. Jampol LM, Acheson R, Eagle RC, et al. Calcification of Bruch's membrane in angioid streaks with homozygous sickle cell disease. *Arch Ophthalmol*. 1987;105:93–98. https://doi.org/10.1001/archopht.1987.01060010099039.
32. Chang AA, Zhu M, Billson F. The interaction of indocyanine green with human retinal pigment epithelium. *Invest Ophthalmol Vis Sci*. 2005;46:1463–1467. https://doi.org/10.1167/iovs.04-0825.
33. Tam J, Liu J, Dubra A, Fariss R. In vivo imaging of the human retinal pigment epithelial mosaic using adaptive optics enhanced indocyanine green ophthalmoscopy. *Invest Ophthalmol Vis Sci*. 2016;57:4376–4384. https://doi.org/10.1167/iovs.16-19503.
34. Bertazzo S, Gentleman E, Cloyd KL, et al. Nano-analytical electron microscopy reveals fundamental insights into human cardiovascular tissue calcification. *Nat Mater*. 2013;12:576–583. https://doi.org/10.1038/nmat3627.
35. Malmberg P, Nygren H. Methods for the analysis of the composition of bone tissue, with a focus on imaging mass spectrometry (TOF-SIMS). *Proteomics*. 2008;8:3755–3762. https://doi.org/10.1002/pmic.200800198.
36. Ralph D, van de Wetering K, Uitto J, Li Q. Inorganic pyrophosphate deficiency syndromes and potential treatments for pathologic tissue calcification. *Am J Pathol*. 2022;192:762–770. https://doi.org/10.1016/j.ajpath.2022.01.012.
37. Arya S, Emri E, Synowsky SA, et al. Quantitative analysis of hydroxyapatite-binding plasma proteins in genotyped individuals with late-stage age-related macular degeneration. *Exp Eye Res*. 2018;172:21–29. https://doi.org/10.1016/j.exer.2018.03.023.
38. Pilgrim MG, Marouf S, Fearn S, et al. Characterization of calcium phosphate spherical particles in the subretinal pigment epithelium–basal lamina space in aged human eyes. *Ophthalmol Sci*. 2021;1:100053. https://doi.org/10.1016/j.xops.2021.100053.
39. Tan ACS, Pilgrim MG, Fearn S, et al. Calcified nodules in retinal drusen are associated with disease progression in age-related macular degeneration. *Sci Transl Med*. 2018;10:eaat4544. https://doi.org/10.1126/scitranslmed.aat4544.
40. Bergen AA, Arya S, Koster C, et al. On the origin of proteins in human drusen: The meet, greet and stick hypothesis. *Prog Retin Eye Res*. 2019;70:55–84. https://doi.org/10.1016/j.preteyeres.2018.12.003.
41. Edwards MM, McLeod DS, Shen M, et al. Clinicopathologic findings in three siblings with geographic atrophy. *Invest Ophthalmol Vis Sci*. 2023;64:2. https://doi.org/10.1167/iovs.64.3.2.
42. Risseeuw S, Ossewaarde-van Norel J, Klaver CCW, et al. Visual acuity in pseudoxanthoma elasticum. *Retina*. 2019;39:1580–1587. https://doi.org/10.1097/iae.0000000000002173.
43. Naouri M, Boisseau C, Bonicel P, et al. Manifestations of pseudoxanthoma elasticum in childhood. *Br J Dermatol*. 2009;161:635–639. https://doi.org/10.1111/j.1365-2133.2009.09298.x.
44. Klein BA. Angioid streaks; a clinical and histophathologic study. *Am J Ophthalmol*. 1947;30:955–968. https://doi.org/10.1016/0002-9394(47)90648-X.
45. Hagedoorn A. Angioid streaks. *Arch Ophthalmol*. 1939;21:935–965.
46. Verhoeff FH. Histological findings in a case of angioid streaks. *Br J Ophthalmol*. 1948;32:531–544. https://doi.org/10.1136/bjo.32.9.531.
47. Chong NHV, Keonin J, Luthert PJ, et al. Decreased thickness and integrity of the macular elastic layer of Bruch's membrane correspond to the distribution of lesions associated with age-related macular degeneration. *Am J Pathol*. 2005;166:241–251. https://doi.org/10.1016/S0002-9440(10)62248-1.
48. Gheduzzi D, Sammarco R, Quaglino D, et al. Extracutaneous ultrastructural alterations in pseudoxanthoma elasticum. *Ultrastruct Pathol*. 2003;27:375–384.
49. Gorgels TGMF, Teeling P, Meeldijk JD, et al. Abcc6 deficiency in the mouse leads to calcification of collagen fibers in Bruch's membrane. *Exp Eye Res*. 2012;104:59–64.
50. Pilgrim MG, Lengyel I, Lanzirotti A, et al. Subretinal pigment epithelial deposition of drusen components including hydroxyapatite in a primary cell culture model. *Invest Ophthalmol Vis Sci*. 2017;58:708–719. https://doi.org/10.1167/iovs.16-21060.
51. Thompson RB, Reffatto V, Bundy JG, et al. Identification of hydroxyapatite spherules provides new insight into subretinal pigment epithelial deposit formation in the aging eye. *Proc Natl Acad Sci U S A*. 2015;112:1565–1570. https://doi.org/10.1073/pnas.1413347112.
52. Szmacinski H, Hegde K, Zeng HH, et al. Imaging hydroxyapatite in sub-retinal pigment epithelial deposits by fluorescence lifetime imaging microscopy with tetracycline staining. *J Biomed Opt*. 2020;25:1–11. https://doi.org/10.1117/1.jbo.25.4.047001J.
53. Lengyel I, Tufail A, Al Hosaini H, et al. Association of drusen deposition with choroidal intercapillary pillars in the aging human eye. *Invest Ophthalmol Vis Sci*. 2004;45:28862892. https://doi.org/10.1167/iovs.03-1083.
54. Kozák E, Bartstra JW, de Jong PA, et al. Plasma level of pyrophosphate is low in pseudoxanthoma elasticum owing to mutations in the ABCC6 gene, but it does not correlate with ABCC6 genotype. *J Clin Med*. 2023;12. https://doi.org/10.3390/jcm12031047.
55. Jansen RS, Duijst S, Mahakena S, et al. ABCC6-mediated ATP secretion by the liver is the main source of the mineralization inhibitor inorganic pyrophosphate in the systemic circulation-brief report. *Arterioscler Thromb Vasc Biol*. 2014;34:1985–1989. https://doi.org/10.1161/ATVBAHA.114.304017.
56. Brinks J, van Dijk EHC, Klaassen I, et al. Exploring the choroidal vascular labyrinth and its molecular and structural roles in health and disease. *Prog Retin Eye Res*. 2022;87:100994. https://doi.org/10.1016/j.preteyeres.2021.100994.
57. Fryczkowski AW. Anatomical and functional choroidal lobuli. *Int Ophthalmol*. 1994;18:131–141. https://doi.org/10.1007/BF00915961.
58. Choi WJ, Mohler KJ, Potsaid B, et al. Choriocapillaris and choroidal microvasculature imaging with ultrahigh speed OCT angiography. *PLOS ONE*. 2013;8:e81499. https://doi.org/10.1371/journal.pone.0081499.
59. Weiter JJ, Ernest JT. Anatomy of the choroidal vasculature. *Am J Ophthalmol*. 1974;78:583–590. https://doi.org/10.1016/S0002-9394(14)76294-4.

60. Olver JM. Functional anatomy of the choroidal circulation: Methyl methacrylate casting of human choroid. *Eye (Lond)*. 1990;4:262−272. https://doi.org/10.1038/eye.1990.38.
61. Federman JL. The fenestrations of the choriocapillaris in the presence of choroidal melanoma. *Trans Am Opthalmol Soc*. 1982;80:498−516.
62. Kozák E, Fülöp K, Tőkési N, et al. Oral supplementation of inorganic pyrophosphate in pseudoxanthoma elasticum. *Exp Dermatol*. 2022;31:548−555. https://doi.org/10.1111/exd.14498.
63. Bartstra JW, de Jong PA, Kranenburg G, et al. Etidronate halts systemic arterial calcification in pseudoxanthoma elasticum. *Atherosclerosis*. 2020;292:37−41. https://doi.org/10.1016/j.atherosclerosis.2019.10.004.
64. Kranenburg G, de Jong PA, Bartstra JW, et al. Etidronate for prevention of ectopic mineralization in patients with pseudoxanthoma elasticum. *J Am Coll Cardiol*. 2018;71:1117−1126. https://doi.org/10.1016/j.jacc.2017.12.062.
65. Spaide RF. Peau d'orange and angioid streaks: manifestations of Bruch membrane pathology. *Retina*. 2015;35:392−397. https://doi.org/10.1097/IAE.0000000000000420.
66. Chen L, Zhang X, Liu B, et al. Age-related scattered hypofluorescent spots on late-phase indocyanine green angiography: the multimodal imaging and relevant factors. *Clin Exp Ophthalmol*. 2018;46:908−915. https://doi.org/10.1111/ceo.13306.
67. Chen L, Yang P, Curcio CA. Visualizing lipid behind the retina in aging and age-related macular degeneration, via indocyanine green angiography (ASHS-LIA). *Eye (Lond)*. 2022;36:1735−1746. https://doi.org/10.1038/s41433-022-02016-3.
68. Marchese A, Rabiolo A, Corbelli E, et al. Ultra-widefield imaging in patients with angioid streaks secondary to pseudoxanthoma elasticum. *Ophthalmol Retina*. 2017;1:137−144. https://doi.org/10.1016/j.oret.2016.10.005.
69. Borrelli E, Uji A, Toto L, et al. In vivo mapping of the choriocapillaris in healthy eyes: a widefield swept-source OCT angiography study. *Ophthalmol Retina*. 2019;3:979−984. https://doi.org/10.1016/j.oret.2019.05.026.
70. Elmer Sevringhaus BL. Postmortem acidity. I. The acids formed in autolyzing liver. *J Biol Chem*. 1923;57:181−189. https://doi.org/10.1016/S0021-9258(18)85537-5.
71. Pan HB, Darvell BW. Calcium phosphate solubility: the need for re-evaluation. *Cryst Growth Des*. 2009;9:639−645. https://doi.org/10.1021/cg801118v.